Microchimica Acta
https://doi.org/10.1007/s00604-018-3158-y

ORIGINAL PAPER

Superlattice stacking by hybridizing layered double hydroxide nanosheets with layers of reduced graphene oxide for electrochemical simultaneous determination of dopamine, uric acid and ascorbic acid

Muhammad Asif[1,2] · Ayesha Aziz[1] · Haitao Wang[1] · Zhengyun Wang[1] · Wei Wang[1] · Muhammad Ajmal[1] · Fei Xiao[1] · Xuedong Chen[2] · Hongfang Liu[1]

Received: 13 September 2018 / Accepted: 7 December 2018

Abstract

A self-assembled periodic superlattice material was obtained by integrating positively charged semiconductive sheets of a Zn-NiAl layered double hydroxide (LDH) and negatively charged layers of reduced graphene oxide (rGO). The material was used to modify a glassy carbon electrode which then is shown to be a viable sensor for the diagnostic parameters dopamine (DA), uric acid (UA) and ascorbic acid (AA). The modified GCE displays excellent electrocatalytic activity towards these biomolecules. This is assumed to be due to the synergistic effects of (a) excellent interfacial electrical conductivity that is imparted by direct neighboring of conductive rGO to semiconductive channels of LDHs, (b) the superb intercalation feature of LDHs, and (c) the enlarged surface with an enormous number of active sites. The biosensor revealed outstanding electrochemical performances in terms of selectivity, sensitivity, and wide linear ranges. Typically operated at working potentials of −0.10, +0.13 and + 0.27 V vs. saturated calomel electrode, the lower detection limits for AA, DA and UA are 13.5 nM, 0.1 nM, and 0.9 nM, respectively, at a signal-to-noise ratio of 3. The sensor was applied to real-time tracking of dopamine efflux from live human nerve cells.

Keywords Direct neighboring · Controllable co-feeding protocol · Zn-NiAl LDH/rGO · Cyclic voltammetry · Differential pulse voltammetry · Live cells · Urine sample

Introduction

Early stage diagnosis of Parkinson's disease (PD) is urgently desirable as effective therapeutic strategies to enhance the efficacy of medical treatments. Dopamine (DA), uric acid (UA) and ascorbic acid (AA) are the functional biomolecules involved in several physiological processes as well as crucial biomarkers for early PD diagnosis [1]. Because of their analogous properties, selective determination of DA, UA, and AA, as well as their simultaneous determination have attracted wealth of attention in biomedical chemistry and diagnostic researches [2]. It is more challenging to determine exact concentrations of these biomolecules owing to their almost similar oxidation potentials on conventional electrodes which result in feeble selectivity [3]. Considering the co-existence of these biological molecules in human body, constructing a highly accurate and sensitive method for simultaneous detection of DA, UA and AA is incredibly important for clinical diagnostics, pathological analysis and to be aware

Muhammad Asif and Ayesha Aziz contributed equally to this work.

Electronic supplementary material The online version of this article (https://doi.org/10.1007/s00604-018-3158-y) contains supplementary material, which is available to authorized users.

✉ Fei Xiao
xiaofei@hust.edu.cn

✉ Xuedong Chen
chenxd@hust.edu.cn

✉ Hongfang Liu
liuhf@hust.edu.cn

[1] Key Laboratory for Large-Format Battery Materials and System, Ministry of Education, Hubei Key Laboratory of Material Chemistry and Service Failure, School of Chemistry and Chemical Engineering, Huazhong University of Science and Technology, Wuhan 430074, People's Republic of China

[2] State Key Laboratory of Digital Manufacturing Equipment and Technology, Huazhong University of Science and Technology, Wuhan 430074, People's Republic of China

Published online: 09 January 2019

of neuronal functions [4]. To date, various methodologies including calorimetry, ionic chromatography, capillary electrophoresis and chemiluminescence have been explored for sensitive detection of these biological fluids [5]. Beside these well-reputed techniques, DA, UA and AA being inherently electroactive have promoted electrochemical transducer based methods for real-time in vivo monitoring of these targets [6, 7]. As is well known, the electrochemical signal intensities of these analytes have extreme reliabilities on sensing elements but it is considerable challenge to detect DA, UA and AA simultaneously for their almost similar oxidation potentials.

Electrochemical biosensors based on tailored nanomaterials such as noble metals, aptamers and enzymes possess the ability of well differentiating oxidation peaks of these biological fluids and physiological recognition species. In addition, they can impart excellent sensitivity and selectivity [8, 9]. However, the scarcity and high cost of these precious noble metals along with natural enzymes suffering from instability, denaturation and complicated immobilization [10, 11] have prevented them practically to be used on large scale in electrochemical sensor systems. As a result, the urgent requirement is undoubtedly the creation of effective electrocatalytic materials composed of nonprecious metals with promising catalytic abilities under such electrochemical conditions. Particularly, low-cost *3d* transition metal oxides/hydroxides possess marvelous electrocatalytic capabilities as well as high stability and hold worth aptitude in electrocatalysis systems [12, 13].

Layered double hydroxides (LDHs) belong to the class of inorganic materials, affording tunable heterogeneous metal cations and interlayer space presenting accessibility of exchangeable charge balancing anions species, have been employed as potential electrode materials in catalysis, [14] separation and biosensing platform [15]. The exfoliation of LDH crystallites into single layer macromolecular arrangement is one of the intriguing features of LDHs, ultimately creating 2D anisotropy of cationic nanosheets [16]. In particular, the fabrication of LDH based efficient electrocatalyst has been restricted owing to highly insulating nature of nonprecious (Fe, Co, Ni, Mn) metal oxides/hydroxides [17]. To overcome this challenge, it is envisioned to hybridize conductive substrates with a single layer of ultrathin LDH nanosheets of transition metals layer by layer on a molecular-scale. This may be a viable approach to achieve overall superior electrochemical performance. Specifically, rGO with extreme high specific surface area and superb electrical conductivity may serve as conductive paths to enrich charge carriers during catalytic reactions. Furthermore, if periodic superlattice composites of cationic LDH nanosheets with anionic graphene oxide layers in alternating sequence are synthesized by face-to face restacking strategy, a boosted synergistic effect empowering fast electron transport in redox processes can be expected. To the best of our knowledge, there is no report on successful fabrication of Zn-NiAl LDH/rGO superlattice to date. The synthesis of Zn-NiAl LDH/rGO superlattice is more challenging than CoAl and other LDHs might be due to the less tendency of NiAl LDH to form huge sized 2D sheets, which would decrease the possibility of face-to-face interaction.

Herein, we describe a controllable co-feeding protocol to harvest heterostacked self-assembly of true Zn-NiAl LDH/rGO superlattice as presented in Fig. 1. Our Zn-NiAl LDH/rGO superlattice can be recovered in powdered form by freeze drying avoiding any agglomeration or demolition of structure.

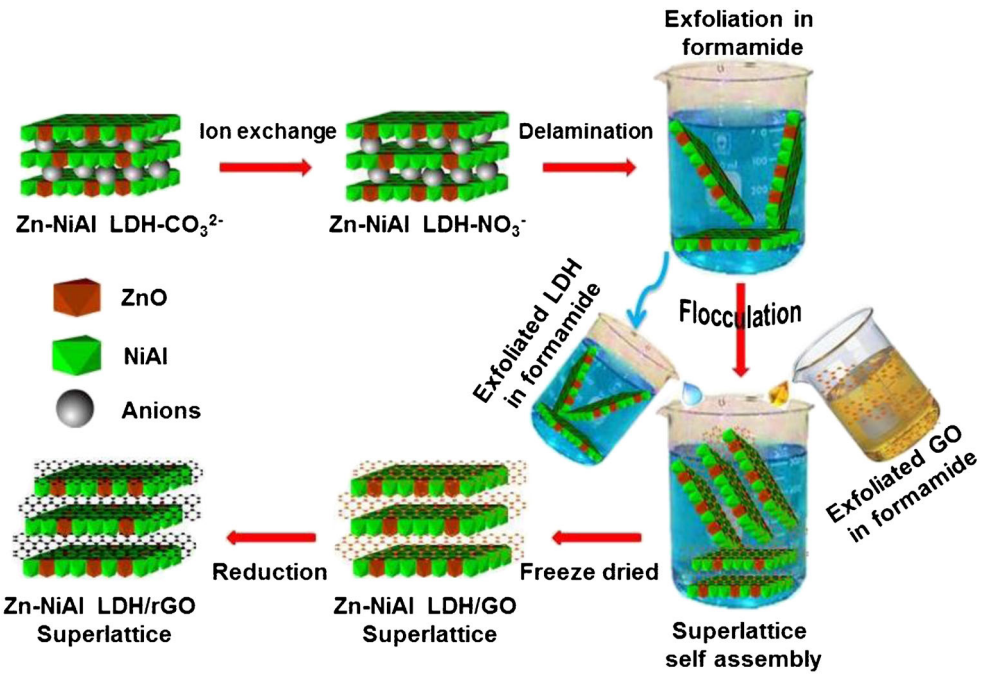

Fig. 1 Schematic illustration of various steps involving in the preparation of Zn-NiAl LDH/rGO superlattice composites

As a proof of concept, Zn-NiAl LDH/rGO superlattice based electrochemical biosensor has been fabricated and demonstrated amazing performance such as wide linear range and low detection limit in ultrasensitive simultaneous detection of AA, UA and DA, and its practical application has been explored for in vitro tracking of DA in live human nerve cells as PD diagnosis.

Materials and methods

Materials and instruments

$Zn(NO_3)_2{\cdot}6H_2O$, $Ni(NO_3)_2{\cdot}6H_2O$, $Al(NO_3)_3{\cdot}9H_2O$, Na_2CO_3, urea, glucose, tyramine, tryptamine, histamine, DA, AA, UA cell culture medium (DMEM), highly concentrated K^+ buffer to stimulate DA from live cells and natural graphite were purchased from Sinopharm Group Chemical Reagent Co, Ltd. Shanghai, China (http://shreagent.lookchem.com/) and (http://www.reagent.com.cn) and used without further purifications. Supporting electrolyte used was 0.1 M phosphate buffer (PB, pH 7.4) comprising of NaH_2PO_4 and Na_2HPO_4 in an appropriate proportion. Typically 0.1 M solution of Na_2HPO_4 was prepared by dissolving 35.8 g of it into 1000 mL of doubly distilled (DD) water and 0.1 M solution of NaH_2PO_4 by dissolving 3.9 g of it into 250 mL of DD water. Then finally, 810 mL of 0.1 M Na_2HPO_4 and 190 mL of 0.1 M NaH_2PO_4 were mixed according to 81/19 proportion and pH was adjusted. X-ray diffraction (XRD) was performed out on a Rigaku D/max-r A diffractometer (Japan) using Cu Ka radiation (40 kV, 200 mA) with a Ni filter, X-ray photoelectron spectroscopy (XPS) was carried on an AXIS-ULTRA DLD-600W X spectrometer and Field-emission scanning electron microscope (FSEM) was acquired on HITACHI X-650 FSEM (Hitachi Co., Japan). Transmission electron microscopy (TEM) and high-resolution transmission electron microscopy (HRTEM) images were achieved by TECNAI G220 U-Twin instrument (Netherlands). The entire electrochemical measurements were carried out on CHI760 electrochemical workstation (CH Instrument Company, Shanghai, China) equipped with saturated calomel electrode, platinum wire and glassy carbon electrode (GCE) as reference, counter and working electrode in typical three electrode system. The self-prepared electrochemical cell was employed. A glass cell covered with lid having four holes through which three electrodes were immersed into cell and fourth hole was used for N_2 purging when necessary. The electrodes were fixed in their particular holes and finally lid was fixed on the tope of cell. The 10 mL N_2 purged PB was poured into cell and electrochemical measurements were conducted with Zn-NiAl LDH/rGO/GCE. All the cyclic voltammetry (CV) and differential pulse voltammetry (DPV) measurements were executed in deoxygenated 0.1 M phosphate buffer (PB) (pH = 7.4) under room temperature and working potential window of −0.4 V to 0.8 V respectively. Electrochemical impedance spectroscopy (EIS) was performed by applying frequency ranges of 1 Hz to 100,000 Hz and sine AC voltage of 0.005 V.

Cell culture and differential pulse voltammetric (DPV) monitoring of DA stimulated

The human neuronal functioning neuroblastoma cell line (SH-SY 5Y) was received from the American Type Culture Collection (ATCC, Manassas, VA, USA). The live SH-SY 5Y cells were cultured in Dulbecco's Modified Eagle Medium (DMEM), supplemented with 10% Fetal Bovine Serum (FBS), 100 units mL^{-1} penicillin and 100 mg mL^{-1} streptomycin by incubating at 37 °C, 5% CO_2 with continued passages. After several passages, the cells with 80% confluency were planted in 6-well plate for real-time detection of extracellular DA levels. Hence the Zn-NiAl LDH/rGO modified GCE (Zn-NiAl LDH/rGO/GCE) was immersed in living cells in 6-well plate at 37 °C for monitoring ubiquitous DA in cells after being triggered by the addition of different spikes of 2.5 M K^+ buffer (stock solution 2.5 M KCl in 0.1 M PB) as stimulus [18].

Synthesis of Zn-NiAl layered double hydroxide (LDH) precursor and ion exchange treatment

The crystalline powdered precursor of the Zn-NiAl LDH with CO_3^{2-} interlayer ions was first synthesized by hydrothermal approach according to our previous work [19]. Briefly, an aqueous solution consisting of 1 mM $Zn(NO_3)_2{\cdot}6H_2O$, 5 mM $Ni(NO_3)_2{\cdot}6H_2O$, 2.5 mM $Al(NO_3)_3{\cdot}9H_2O$ and 25 mM urea was poured into Teflon-lined autoclave and kept at 100 °C for 24 h. After the autoclave cooled down naturally, the precipitates were collected, washed with deionized (DI) water for five times and finally dried at 45 °C overnight.

The ion exchange treatment was carried out to prepare Zn-NiAl LDH with NO_3^- counter ions. Typically, 0.8 g of Zn-NiAl LDH-CO_3^{2-} was mixed homogeneously in 800 mL of N_2 saturated aqueous solution comprising of 1.5 M $NaNO_3$ and 5 mM HNO_3 and kept on mechanical shaker at 130 rpm for 24 h at ambient temperature. Finally, washing and centrifugation of Zn-NiAl LDH-NO_3^- was done in N_2 saturated DI water prior to freeze drying.

Exfoliation of Zn-NiAl LDH and graphene oxide (GO) precursors

To achieve exfoliated nanosheets of Zn-NiAl LDH, continuous mechanical shaking was carried out in formamide. Typically, 50 mg Zn-NiAl LDH-NO_3^- was dispersed in 150 mL of formamide and kept on mechanical shaker at

130 rpm for 60 h. The supernatant was separated after centrifuging at 4000 rpm for 10 min provided the centrifugational force of 1792 rcf.

Graphene oxide (GO) sheets were prepared by modified Hummers method [20]. The key point of our new methodology is to execute exfoliation of GO in DMF rather than frequently used water. Briefly, 80 mL DMF containing 25 mg GO was treated by intensive sonication for 8 h. After centrifugation at 12000 rpm provided with centrifugational force of 16,128 rcf, the supernatant was obtained and diluted to 150 mL by formamide under constant stirring.

Controllable co-feeding protocol to fabricate Zn-NiAl LDH/GO superlattice

We control the experimental conditions during co-feeding protocol to harvest heterostacked self-assembly of true Zn-NiAl LDH/GO superlattice nanohybride. In a typical procedure, 150 mL of each Zn-NiAl LDH and GO supernatant solution was added dropwise at a controlled speed of 1.5 mL min^{-1} into another 200 mL formamide solution with continuous stirring. The process of stirring was continued for further 2 h after controllably adding the two feed solutions. The product was centrifuged and washed repeatedly with ethanol and water and then freeze-dried to recover superlattice composites. Similarly, Zn-NiAl LDH/GO/ direct mixing was also synthesized using same amount of Zn-NiAl LDH and GO supernatant solutions. Without using formamide as solvent, Zn-NiAl LDH was mixed by dropwise adding into stirring GO suspension and continuously stirred for further 2 h. Then 40 mg of Zn-NiAl LDH/GO was kept in a container and then this container was placed in another vessel having 500 μl of hydrazine (85%) to avoid direct contact of Zn-NiAl LDH/GO and hydrazine. Under this procedure, GO species was reduced by hydrazine, and Zn-NiAl LDH/reduced GO (rGO) composite was obtained. This air tight container was placed at 90 °C for 12 h to get Zn-NiAl LDH/rGO superlattice. Under same conditions, other control samples were also fabricated as shown in Table S1.

Preparation of working electrode

To get modified GCE, firstly the surface of GCE (3 mm diameter) was cleaned by polishing with 0.3 and 0.05 μm alumna slurry on microcloth pads and then rinsed with doubly distilled (DD) water. Then, DD water and ethanol were used to wash GCE ultrasonically and dried under N_2 purging. A homogeneous mixture of 3 mg of Zn-NiAl LDH/rGO superlattice in 1 mL of DD water was prepared under vigorous stirring. Secondly, 5 μl of above suspension was cast on thoroughly polished surface of GCE and dried at ambient temperature to evaluate analytical performances. The other control materials were also casted on GCE under same procedure.

Choice of materials

The choice of materials always remains an important task for researchers to achieve superior catalytic activity. Among the transition metals, Ni possesses improved electrocatalytic ability for redox reactions owing to Ni^{2+}/Ni^{3+} redox couple on electrode surface, inexpensiveness, good mechanical strength and electron transferring capability [21]. The filling of *d* orbital is the reason behind enhanced catalytic activity of Ni centers. The band theory reveals the bonding that is derived by interacting cations and valence electrons. Therefore, the overlapping in transition metals occurs between *s* orbital and *d* orbital which affects the filling of *d* electrons. Only eight electrons can enter in *3d* band of Ni rather than entering ten electrons after entirely filling of *4 s* due to the band overlapping of *4 s* orbital and *3d* creates band holes. The existence of these band holes makes the metals to be capable of accepting electrons from outside and absorbing species by band construction which as a result upsurge catalytic properties [22]. From Fig. S5, it is revealed that the presence of ZnO species in Zn-NiAl LDH largely enhances the electroactive surface area and therefore the sensitivity for electrochemical sensing system. Its enhanced surface area facilitates electron transfer and increases adsorption strength toward biomolecules. In this work, we preferred to harvest alternatively stacked assembly of delaminated Zn-NiAl LDH nanosheets and rGO layers in superlattice form instead of using direct mixing of two materials without exfoliation. The insertion of extremely conductive rGO layers in between the interlayer spaces of LDH is probably accomplished by mixing exfoliated nanosheets of both materials with controllable co-feeding protocol and these inserted rGO layers consequently increases electron transportation. The following is the expected possible catalytic mechanism;

$$Ni^{2+} + OH^- \longrightarrow Ni^{3+} + H_2O + e^- \quad (1)$$

$$Ni^{3+} + (AA, DA, UA) \longrightarrow Ni^{2+} + (\text{Dehydroascorbic acid, Dopaminequinone, Allantoin}) \quad (2)$$

Owing to high-cost of noble metals and poor cycling performance suffered by conducting polymers during long-term stability assays, we avoided to use such kind of materials.

Results and discussion

Characterization of Zn-NiAl LDH/rGO superlattice

The morphologies of prepared superlattice composites have been investigated by SEM and TEM observations. The SEM images of rGO inserted heteroassembled LDHs at different magnifications exhibit that the composite consists typical platelet like hexagonal flakes (Fig. 2a–c), indicating that the well restoration of atomic structure of LDH is achieved during restacking assembly of charged sheets of rGO and LDHs. The platelet like hexagonal morphology of Zn-NiAl LDHs is well maintained after thoroughly completed anion exchange process (Supporting Information, Fig. S1).

Figure 2e and e show the TEM observations of superlattice composites at different magnifications. Due to the electrostatic interaction between oppositely charged sheets, the morphology of platelet like flakes disclosed the possible scenario that rGO nanosheets have been successfully inserted into layers of LDHs. Each period of lamellar fringes with two alternating layers spacing of 0.9 nm in high resolution TEM image speculates to be heterostacked (Fig. 2f), and rules out the probability of anion/solvent inserted in the layers of LDHs. Figure 2g demonstrates SEM-EDX mapping profile of Zn-NiAl LDH/rGO superlattice corresponding to the signals of Zn, Ni, Al, C and O, respectively, in which an even distribution of elements has been observed. These results validate the intimate heteroassembly of LDH monolayers and rGO nanosheets.

The XRD pattern of CO_3^{2-}, NO_3^- and rGO inserted in Zn-NiAl LDH layers has been shown in Fig. 3a. Compared with the basal spacing of 0.75 nm for Zn-NiAl LDH-CO_3^{2-} precursor, the Zn-NiAl LDH-NO_3^- holds an enlarged spacing of 0.85 nm, authenticating the insertion of larger NO_3^- ions in the interlayer space [23].

The XRD measurements of Zn-NiAl LDH/rGO exhibit an interlayer spacing of 0.91 nm, which is consistent with the added up nanosheets thickness of LDH (0.49 nm) and rGO (0.4 nm) and further endorsed by 0.9 nm HRTEM lattice fringes of two alternate layers spacing in heteroassembled composites. It is worth mentioning that a clear diffraction peak of (002) around 21° with basal spacing of (0.54 nm) confirms the evidences for the creation of heteroassembled configuration of LDH/G superlattice. This result exposes the effective-

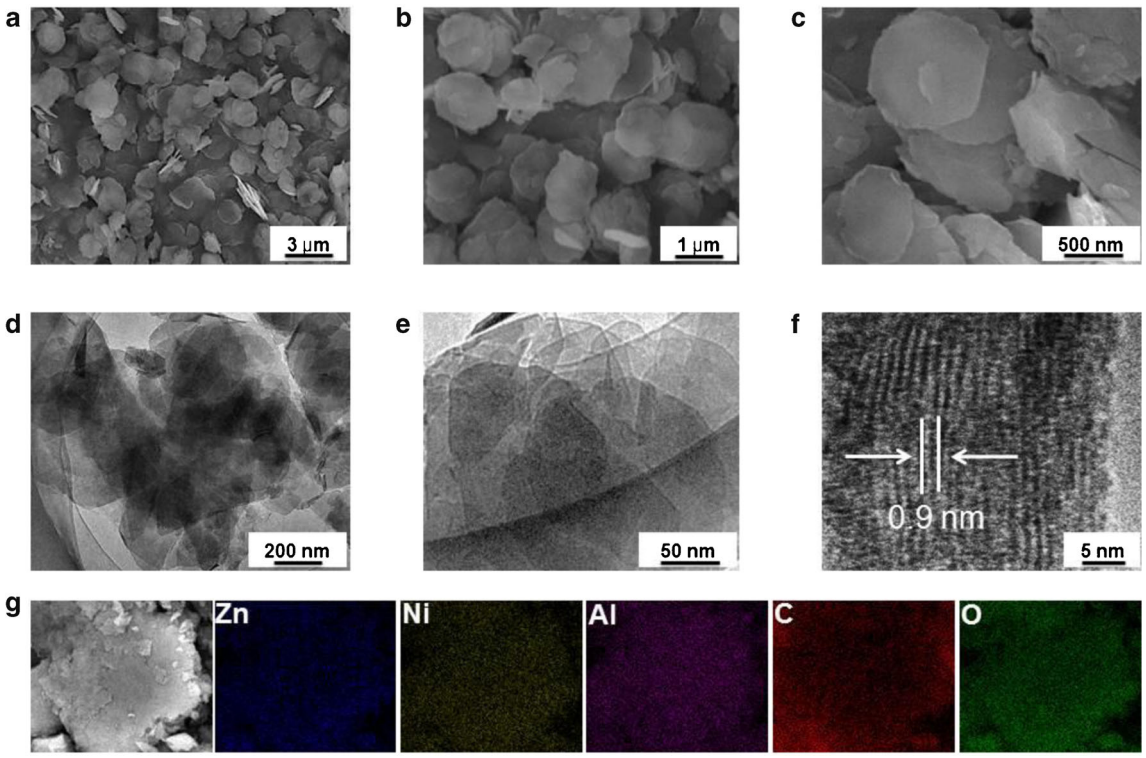

Fig. 2 Structural analysis of self-assembled product, **a**–**c** SEM, **d** and **e** TEM images at different magnifications and **f** HRTEM image, and **g** SEM-EDX mapping results of Zn-NiAl LDH/rGO superlattice composites

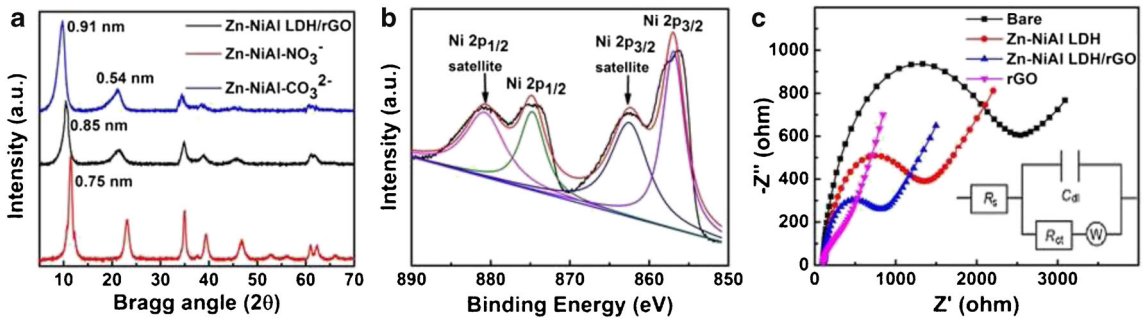

Fig. 3 **a** XRD patterns of Zn-NiAl LDH with CO_3^{2-}, NO_3^- and rGO inserted in between the layers, **b** XPS core level Ni 2p spectra of Zn-NiAl LDH/rGO, and **c** EIS plots of Bare, Zn-NiAl LDH, Zn-NiAl LDH/rGO and rGO electrodes in 0.1 M KCl comprising of 1.0 mM $K_3Fe(CN)_6$ and 1.0 mM $K_4Fe(CN)_6$. Frequency range: 0.1–105 Hz. Inset is the equivalent circuit

ness of our co-feeding protocol because (002) peak is not detected when feeding of two exfoliated solutions is not suitably controlled [24]. In addition, two in-plane diffraction peaks (100) and (110) at around 35° and 60° verify the presence of intact LDH nanosheets in heteroassembled material, confirming the retained 2D structure of LDH nanosheets in superlattice composite. In contrast, when Zn-NiAl LDH solution is directly poured into GO solution, no superlattice composites with alternate stacking assembly can be observed from the diffraction peak of assembled product (Fig. S2), indicating that most of Zn-NiAl LDH nanosheets re-stacked with itself. Figure 3b illustrates core fitting spectrum of Ni $2p_{3/2}$ and Ni $2p_{1/2}$ at 856.3 eV and 874.2 eV along with two satellite peaks and spin energy gap of 17.9 eV, which confirm the presence of Ni^{2+} species in superlattice composites [25, 26]. FTIR spectra of CO_3^{2-}, NO_3^- and rGO intercalated in Zn-NiAl LDH, XPS wide scan and core level Zn 2p spectra of Zn-NiAl LDH/rGO have been inserted in Fig. S3. The XPS survey for C 1 s of reduced graphene oxide in Zn-NiAl LDH/rGO superlattice has been shown in Fig. S4.

Electrochemical performance of Zn-NiAl LDH/rGO hydride electrode

Electrochemical impedance spectroscopy (EIS) has further been employed to measure interfacial charge transfer properties of Zn-NiAl LDH and Zn-NiAl LDH/rGO superlattice modified GCE in $[Fe(CN)_6]^{3-/4-}$ redox probe as depicted by Fig. 3c. Inset is the Randle equivalence circuit equipped with solution resistance (R_s), charge transfer resistance (R_{ct}), double layer capacitance (C_{dl}) and Warburg constant (W). The rGO modified GCE shows a small R_{ct} value of 310 Ω because of its high conductivity as compared with other electrodes. Due to the semiconductive properties of LDHs, the GCE modified by Zn-NiAl LDH has shown larger R_{ct} value of 1318 Ω in comparison with extremely reduced R_{ct} value of 745 Ω exhibited by Zn-NiAl LDH/rGO superlattice. But this value 1318 Ω is still less than bare GCE with R_{ct} of 2455 Ω, demonstrating fractional electron transfer capability due to the existence of holes within the layers of LDHs. The enhanced conductivity presented by superlattice is owing to the fact that rGO layers ensure several small energy gaps, which are liable for interfacial charge transfer ability [27]. Similar results have also been achieved by recording CV curve of different modified electrodes in $[Fe(CN)6]^{3-/4-}$ redox solution (Fig. S5). The electrochemical active surface areas of different electrodes are calculated according to the Randles–Sevcik equation (Supporting Information Fig. S5).

The electrocatalytic performances have been evaluated by cyclic voltammetry (CV) measurements on Zn-NiAl LDH/rGO superlattice composites modified GCE in the absence and presence of target molecules in 0.1 M PB (pH 7.4). As shown in Fig. 4a–c, an enhanced oxidation peak is recorded in the presence of 1 mM AA, where no obvious peak is detected in pure PB alone. For the target molecules of DA, a well-defined pair of redox peaks is appeared corresponding to the oxidation of DA to equinone and subsequently the reduction of equinone to DA [28]. The similar behavior is recorded with UA under same concentration but at different oxidation potential. This excellent electrocatalytic performance may arise from various factors: (i) the insertion of highly conductive rGO sheets as π-electron-rich substrate in LDHs layers to facilitate rapid electron transport (Table S1 and Fig. S6); (ii) the superlattice possesses enlarged surface area; (iii) the target molecules are readily accessible to porous surface of heteroassembled composites; (iv) the structurally integrated charged sheets harvest enormous surface active sites. It is clear that different interaction modes on the surface of superlattice modified GCE have been exposed by structurally different biotic molecules, which guarantee the possibility to achieve the goal for simultaneous detection of AA, DA and UA. In addition, the CV and differential pulse voltammetry (DPV) curves in co-existive system of 0.1 M PB containing 100 μM AA, 40 μM DA and 40 μM UA have been displayed in Fig. 4d–f representing three distinct peaks for simultaneous detection of these biomolecules.

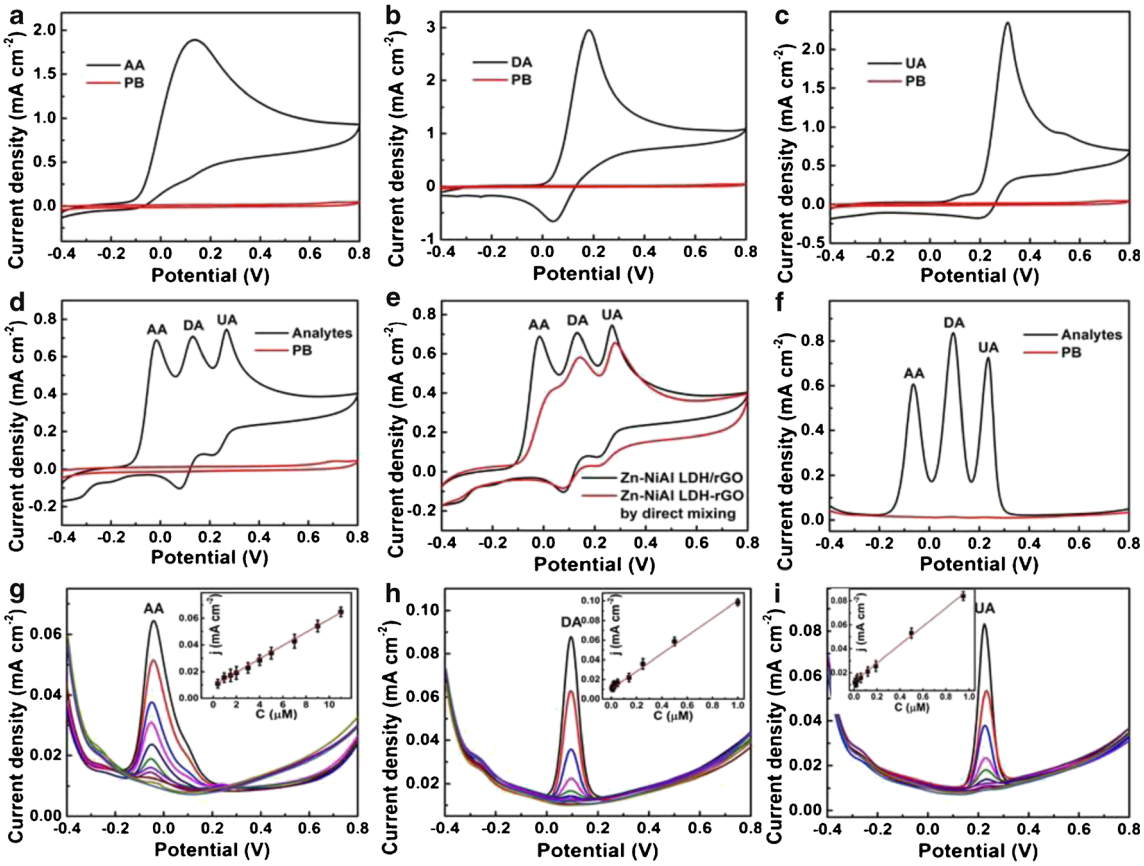

Fig. 4 Electrochemical responses of Zn-NiAl LDH/rGO electrode upon the addition of AA, DA and UA. **a**–**c** typical CV curves in the absence (red line) and presence (black line) of 1 mM AA, DA, and UA, respectively in 0.1 M PB (pH = 7.4). CV curves with (**d**) Zn-NiAl LDH/rGO, (**e**) different modified electrodes, and (F) DPV curves in the presence of mixture of 100 μM AA, 40 μM DA and 40 μM UA, respectively. The DPV curves at different concentrations (**g**) The AA concentrations from 0 to 11 μM. **h** The DA concentrations from 0 to 1 μM. **i** The UA concentrations from 0 to 1 μM respectively. Insets are the calibration plots of current density vs. concentration of each biomolecule. (DPV conditions) Potential window −0.4 V to 0.8 V, Incr E 4 mV, Amplitude 50 mV, Pulse width 0.06 s, Sample width 0.02 s, Pulse period 0.25 s, and Quiet time 2 s, (The number of experiments performed, $n = 6$)

The ability of directly mixed Zn-NiAl LDH-rGO nanohybrid and Zn-NiAl LDH/rGO superlattice modified GCEs to differentiate the signal peaks in co-existence system of these analytes is also observed by CV measurements (Fig. 4e). Moreover, the electrocatalytic activities of Zn-NiAl LDH/rGO, Zn-NiAl LDH, rGO modified GCEs and bare GCE have been compared under the same condition (Fig. S7). Benefited from the synergistic effect between inserted π-electron-rich rGO and semiconductive channels of LDHs, Zn-NiAl LDH/rGO superlattice electrode has exhibited intriguing performances in terms of well-separated peaks. DPV being more sensitive, eliminating non Faradic current gives improved analytical signal compared with CV, due to which remarkable distinction in peaks has been observed and this superb performances may be owing to large surface area providing fast electron transfer kinetics and also enables rapid adsorption of biomolecules [8]. DPV curves for different concentrations of AA, DA and UA along with corresponding linear slopes (inset) at Zn-NiAl LDH/rGO superlattice electrode have been illustrated in Fig. 4g–i. Because of containing aromatic ring in their structures, the oxidation peak current densities for DA (0.098 mA cm^{-2}) and UA (0.085 mA cm^{-2}) are much larger than AA (0.017 mA cm^{-2}) at 1 μM. The enlarged DPV curves of DA and UA at low concentrations are given in Fig. S8. Thus, the enhanced interaction of DA on Zn-NiAl LDH/rGO material may possibly be owing to the fact of π or ring stacking collaborations between DA and the aromatic domains of Zn-NiAl LDH/rGO nanocomposites [29]. The detection limits (LOD) of 13.5 nM for AA, 0.1 nM for DA and 0.9 nM for UA have been achieved with signal-to-noise ratio ($S/N = 3$), which are lower than most of previously reported electrochemical biosensors (Table 1).

The simultaneous detection of different biomarkers with marvelous sensitivity and selectivity during co-existence of AA, DA and UA in various biological systems is of extreme mandatory. In these measurements, the concentration of target component is varied while the other two biomolecules are held at fixed concentrations. As shown in Fig. 5a, three distinct

Table 1 Summary of previously published results for detection of UA, DA, and AA by DPV using different electrode materials

Electrode materials	Linear range (μM)			Detection limit (nM)			Ref.
	AA	DA	UA	AA	DA	UA	
ZnO NWs arrays on 3D hierarchical graphene	1–100	0.1–50	0.1–60	100	1	1	[1]
Hierarchical nanoporous PtTi alloy	200–1000	4–500	1–1000	24200	3200	5300	[30]
rGO incorporated $_{L}$-lysine	100–1200	2–60	20–200	2000	100	150	[31]
Graphene-zinc oxide composite	50–2350	3–330	1–70	3710	1080	330	[8]
Au NPs anchored N-doped graphene	–	0.03–40	–	–	10	–	[32]
Metalloporphyrin with graphene sheet	–	0.01–200	–	–	1.4	–	[33]
Graphene solution-gated transistors	–	–	–	1000	1	10000	[34]
Zn-NiAl LDH/rGO superlattice	0.5–11	0.001–1	0.0011–0.95	13.5	0.1	0.9	This work

peaks are located corresponding to different analytes, in which AA concentration is changed from 0 to 75 μM with LOD of 4 μM, at fixed concentrations of DA (10 μM) and UA (10 μM). Almost constant oxidation current density values for DA and UA are observed as the concentration of target component AA is increased. Similar trends are established upon successive additions of DA and UA from 0 to 40 μM for each with LODs of 0.4 μM and 0.48 μM respectively with $S/N = 3$ when other two biomolecules are kept at constant concentrations (Fig. 5b and c). The linear curves for each of the components have been inserted in the inset of respective figures. The outstanding electrochemical sensing abilities of Zn-NiAl LDH/rGO superlattice electrode in the co-existence of AA, DA and UA are also confirmed by simultaneously detection of three biomolecules and their resultant well separated oxidation peaks increased linearly (Fig. 5d). The calibration plots are linear in proportion to their concentrations (Fig. S9). Selectivity of Zn-NiAl LDH/rGO sensor has also been evaluated in the presence of several potential interferential species such as NaCl, $CaCl_2$, histamine, tyramine, tryptamine, H_2O_2 and glucose that possibly co-exist with these biomolecules in blood. As presented in Fig. 5e, distinct responses are

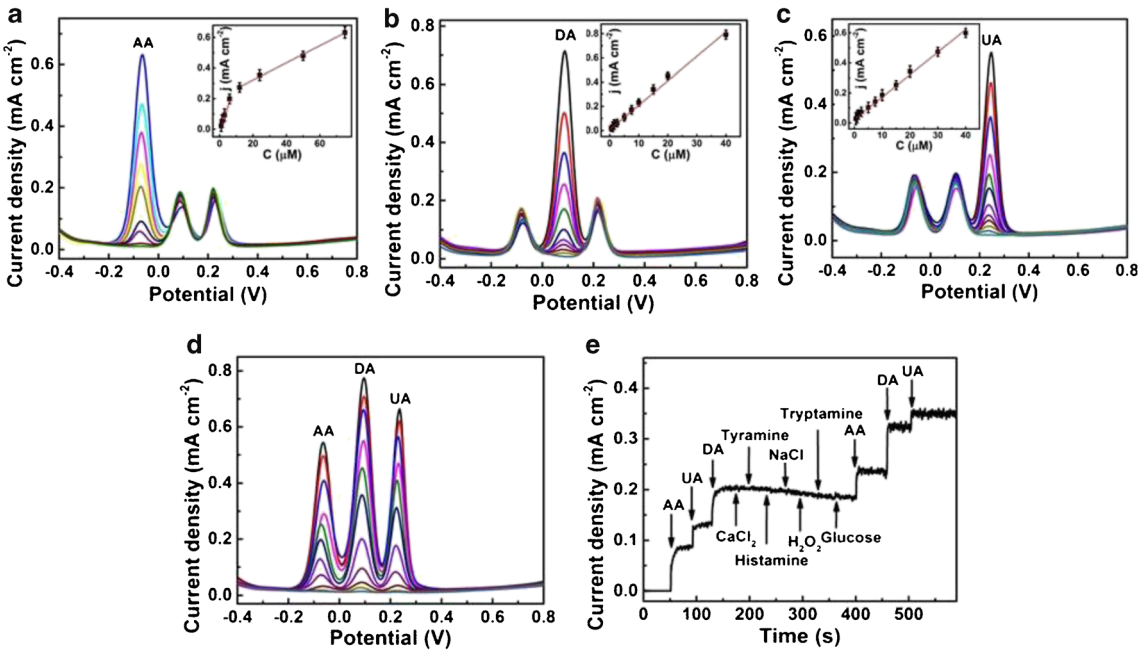

Fig. 5 DPV profiles on Zn-NiAl LDH/rGO electrode in co-existence system AA, DA and UA. DPV profile of (**a**) AA with varied concentrations from 0 to 75 μM in mixture of 10 μM DA and 10 μM UA, (**b**) DA with varied concentrations from 0 to 40 μM in mixture of 24 μM AA and 10 μM UA and (**c**) UA with varied concentrations from 0 to 40 μM in mixture of 24 μM AA and 10 μM DA. Insets are the calibration plots of current density vs. concentration of each biomolecule. DPV profiles in a mixture of AA, DA and UA with different concentrations of each biomolecule (**d**), Amperometric responses of Zn-NiAl LDH/rGO electrode to the addition of 40 μM of AA, DA, UA and 10-folds higher concentration of other interfering species in stirring 0.1 M PB at applied potential of 0.35 V (**e**). (Working potentials of −0.10, +0.13 and + 0.27 V vs. saturated calomel electrode, $n = 6$)

noted upon the successive addition of AA, DA and UA in stirring 0.1 M PB at applied potential of 0.35 V, while no obvious signals are recorded by augmenting 10-folds higher concentration of each interfering substances. The above consequences demonstrate that the fabricated electrode material possesses amazing anti-interfering capabilities.

In-vitro tracking biomolecules from biological fluids

High performance of Zn-NiAl LDH/rGO superlattice electrode unequivocally reveals its promising feasibility for tracking DA released from human neuronal functioning neuroblastoma cell line SH-SY-5Y after being stimulated by highly K^+ buffer. And bright field images of live cell have been shown in Fig. 6a. It has been reported that depolarization of cell membrane caused by the addition of highly concentrated extracellular K^+ buffer, engenders an influx of Na^+ and Ca^{2+} through the opening of Na^+ channels, followed by the opening of Ca^{2+} channels [35]. Consequently, the elevated Ca^{2+} influx evokes numerous proteins to immobilize and hence the fusion of large dense-core vesicles of the cells. The opening voltage-sensitive Ca^{2+} channels upsurges the intracellular level of Ca^{2+} enough to trigger exocytosis, subsequently DA inside fused with cell membrane is released to extracellular region [36]. Moreover, the CCK-8 assay depicts good biocompatibility of superlattice material to living cells in maintaining 98.9%, 96.3%, 93.4%, 91.1% and 89.2% viability upon incubation with Zn-NiAl LDH/rGO electrode for 1 h, 2 h, 3 h, 4 h and 5 h, respectively (Fig. 6b). Figure 6c expresses the DPV recordings of current responses to the oxidation of DA released after being stimulated upon the injection of each spike of concentrated K^+ buffer in the absence and presence of SH-SY-5Y cells and reaches steady-state value within 10 s. Typically, 10 mL of SH-SY-5Y cell solution was present in each well of 6-well plate, when the density of cells had reached 80% confluence. The modified working electrode (Zn-NiAl LDH/rGO/GCE) together with counter and reference electrodes are immersed perpendicularly in cell suspension of one well covering the well with lid. DPV measurements are carried out between −0.1 V to 0.35 V upon the addition of 0.42 mL of 2.5 M K^+ buffer to make the final concentration of 105 mM, 210 mM and 315 mM in same suspension to release DA from cells. It can be noted that upon inoculating each spike of stimulus, no any current signal is detected in the absence of cell, while remarkable current responses are observed in the presence of living cells at peak potential of around +0.093 V. The peak current density values decrease upon successive addition of stimulator due to depletion of cellular dopamine stores. The highest two current density values from the electrochemical responses for each spike are averaged. The current value before the stimulation is defined as the background and is subtracted from the peak current (expressed in DPV) to calculate the actual current values, which are then graphed. These current signals go on decreasing after every spike giving current density of 3.83 μA cm^{-2}, 1.71 μA cm^{-2} and 1.01 μA cm^{-2}, respectively (Fig. 6d). The regression equation has been used to quantify excreted DA concentrations

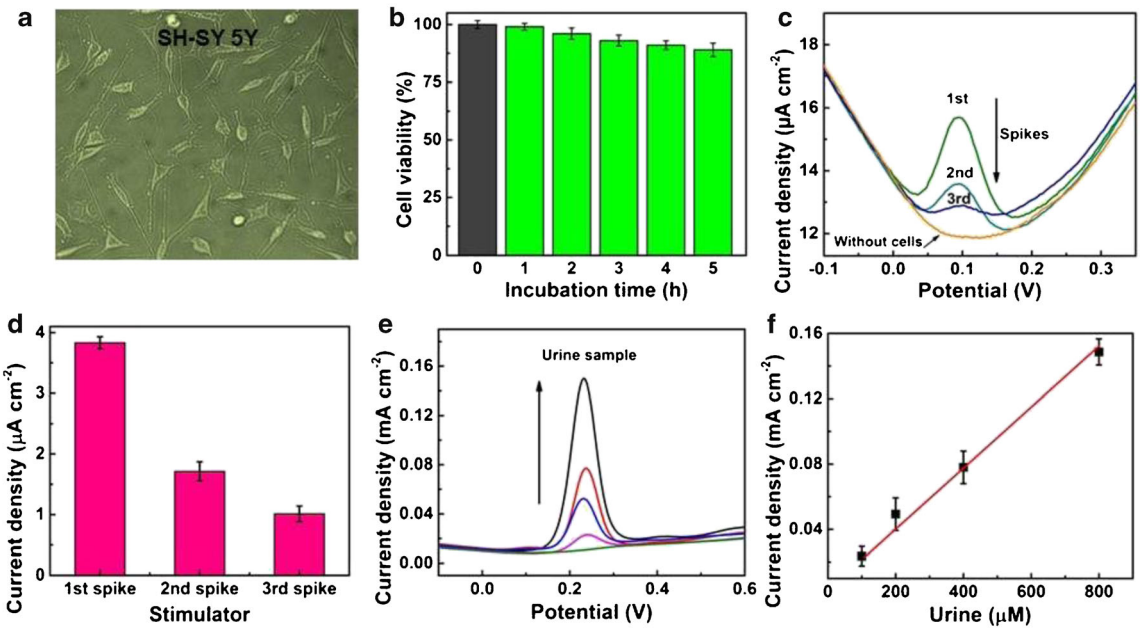

Fig. 6 Bright-field image of neuroblastoma cell line (**a**), Quantitative cell viability results by CCK-8 assay for SH-SY 5Y cells incubated with Zn-NiAl LDH/rGO electrode (**b**), DPV responses of Zn-NiAl LDH/rGO electrode with the addition of different aliquots of stimulator in the absence and presence of neuroblastoma cell line (**c**), The current responses of different spikes of stimulator to living cells (**d**), DPV responses of Zn-NiAl LDH/rGO electrode to different aliquot addition of human urine sample (**e**), The calibration plot of current density vs. spiked concentrations of urine sample (**f**). ($n = 6$)

which are found to be 0.102 μM, 0.05 μM and 0.014 μM respectively. In addition, the results of our biosensor for determination of DA concentrations in live cells have also been compared with conventional colorimetric method. For first spike, 0.11 μM DA is measured by conventional colorimetric method with RSD value of 3.1%. Thus, the aforementioned outcomes undoubtedly validate the reliable presentation of Zn-NiAl LDH/rGO superlattice material for real-time monitoring of DA excretions from live cells.

UA is an important biomarker in diagnosis of various diseases associated with purine metabolism like hyperuricaemia, depression, urolithiasis, gout, cardiac and kidney diseases, and the monitoring of exact level of UA is mandatory to circumvent these lethal disorders.

The current density responses of DPV to the oxidation of UA are also collected upon the addition of certain aliquots of humane urine sample in 10 mL of PB. By injecting each aliquot of urine, the DPV responses go on increasing due to endogenous amounts of UA excreted form urine sample with current density of 0.022 mA cm^{-2}, 0.051 mA cm^{-2} 0.077 mA cm^{-2} and 0.149 mA cm^{-2}, respectively (Fig. 6e). The regression equation has been used to measure excreted UA concentrations which are found to be 0.065 μM, 0.48 μM, 0.91 μM and 2.80 μM respectively. The linear calibration plot of current density vs. spiked concentrations of urine sample has been shown in Fig. 6f. The ubiquitous UA concentration in urine sample has also been detected by conventional calorimetric method and compared with our results. The analytical performance of our electrochemical sensor for the detection of UA from urine sample is found in good agreement with the results obtained by calorimetric method with RSD values of 2.44%. The above mentioned outcomes unequivocally ensure the reliable application of Zn-NiAl LDH/rGO superlattice electrode for DA sensing from live cells along with ubiquitous UA detection from biotic fluids. In this study, no major limitations have been observed, which makes our sensor reliable to be employed for determination of different biomolecules. In our opinion, the small yield of Zn-NiAl LDH/rGO superlattice material during fabrication process is the minor limitation of our method which does not affect the sensing capabilities.

Conclusion

We have developed a genuine superlattice assembly of composite materials by electrostatic interaction between oppositely charged Zn-NiAl LDH nanosheets and rGO layers via controllable co-feeding protocol, in which both exfoliated counterpart constituents are hybridized on molecular-scale in an alternate sequence. The molecular-level hybridization endowed the superlattice with direct neighboring of conductive rGO to semiconductive channels of LDHs, which significantly enhanced the electron transfer capability during electrochemical reaction. Due to the synergistic effect derived from the drastic interfacial conduction caused by integrating electrical properties of rGO nanosheets, the superb intercalation feature of LDHs, and their enlarged surface area with huge surface active sites, the heteroassembled material exhibited excellent electrocatalytic properties. Accordingly, an electrochemical biosensing platform based on Zn-NiAl LDH/rGO superlattice composite has been established for simultaneous detection of AA, DA and UA, which demonstrated outstanding performances towards specific and sensitive detection of these biotic fluids. Moreover, the biosensor has been practically used in real-time monitoring of extracellular DA efflux excreted by live cells after being stimulated by high K^+ solution and endogenous amount of UA from human urine sample. Thus, our structurally integrated heteroassembling strategy of superlattice composites embraces encouraging application potential in biosensing platform and diseases diagnostics.

Acknowledgements National Natural Science Foundation of China (No. 51572094, 51435006), the Innovation Foundation of Huazhong University of Science (No. 2015TS150, 2015ZZGH010) and Technology and the Key Laboratory for Large-Format Battery Materials and System. We acknowledge the support of the Analytical and Testing Center of the Huazhong University of Science and Technology for SEM and XPS measurements.

Compliance with ethical standards The author(s) declare that they have no competing interests.

References

1. Yue HY, Huang S, Chang J, Heo C, Yao F, Adhikari S, Gunes F, Liu LC, Lee TH, Oh ES (2014) ZnO nanowire arrays on 3D hierachical graphene foam: biomarker detection of Parkinson's disease. ACS Nano 8:1639–1646
2. Tavakolian E, Tashkhourian J (2018) Sonication-assisted preparation of a nanocomposite consisting of reduced graphene oxide and CdSe quantum dots, and its application to simultaneous voltammetric determination of ascorbic acid, dopamine and uric acid. Microchim Acta 185:145–152
3. Li Y, Jiang Y, Song Y, Li S (2018) Simultaneous determination of dopamine and uric acid in the presence of ascorbic acid using a gold electrode modified with carboxylated graphene and silver nanocube functionalized polydopamine nanospheres. Microchim Acta 185: 382–391
4. Taleb M, Ivanov R, Bereznev S, Kazemi SH, Hussainova I (2017) Ultra-sensitive voltammetric simultaneous determination of dopamine, uric acid and ascorbic acid based on a graphene-coated alumina electrode. Microchim Acta 184:4603–4610
5. Wang L, Dong Y, Zhang Y, Zhang Z, Chi K, Yuan H, Zhao A, Ren J, Xiao F, Wang S (2016) PtAu alloy nanoflowers on 3D porous ionic liquid functionalized graphene-wrapped activated carbon

fiber as a flexible microelectrode for near-cell detection of cancer. NPG Asia Mater 8:337–345
6. Ghazizadeh AJ, Afkhami A, Bagheri H (2018) Voltammetric determination of 4-nitrophenol using a glassy carbon electrode modified with a gold-ZnO-SiO_2 nanostructure. Microchim Acta 185:296–303
7. Asif M, Aziz A, Ashraf G, Wang Z, Wang J, Azeem M, Chen X, Xiao F, Liu H (2018) Facet-inspired core-shell gold nanoislands on metal oxide octadecahedral heterostructures: high sensing performance toward sulfide in biotic fluids. ACS Appl Mater Interfaces 10:36675–36685
8. Zhang X, Zhang YC, Ma LX (2016) One-pot facile fabrication of graphene-zinc oxide composite and its enhanced sensitivity for simultaneous electrochemical detection of ascorbic acid, dopamine and uric acid. Sens Actua B: Chemical 227:488–496
9. He W, Ding Y, Ji L, Zhang X, Yang F (2017) A high performance sensor based on bimetallic NiCu nanoparticles for the simultaneous determination of five species of biomolecules. Sens Actua B: Chemical 241:949–956
10. Xu Z, Yang L, Xu C (2015) Pt@UiO-66 heterostructures for highly selective detection of hydrogen peroxide with an extended linear range. Anal Chem 87:3438–3444
11. Asif M, Aziz A, Azeem M, Wang Z, Ashraf G, Xiao F, Chen X, Liu H (2018) A review on electrochemical biosensing platform based on layered double hydroxides for small molecule biomarkers determination. Adv Colloid Interf Sci 262:21–38
12. Asif M, Liu H, Aziz A, Wang H, Wang Z, Ajmal M, Xiao F (2017) Core-shell iron oxide-layered double hydroxide: high electrochemical sensing performance of H_2O_2 biomarker in live cancer cells with plasma therapeutics. Biosens Bioelectron 97:352–359
13. Asif M, Haitao W, Shuang D, Aziz A, Zhang G, Xiao F, Liu H (2017) Metal oxide intercalated layered double hydroxide nanosphere: with enhanced electrocatalyic activity towards H_2O_2 for biological applications. Sens Actua B: Chemical 239:243–252
14. Gu F, Cheng X, Wang S, Wang X, Lee PS (2015) Oxidative intercalation for monometallic Ni^{2+}-Ni^{3+}layered double hydroxide and enhanced capacitance in exfoliated nanosheets. Small 11:2044–2050
15. Tel-Vered R, Kahn JS, Willner I (2016) Layered metal nanoparticle structures on electrodes for sensing, switchable controlled uptake/release, and photo-electrochemical applications. Small 12:51–75
16. Wang Q, O'Hare D (2012) Recent advances in the synthesis and application of layered double hydroxide (LDH) nanosheets. Chem Rev 112:4124–4155
17. Zhao MQ, Zhang Q, Huang JQ, Wei F (2012) Hierarchical nanocomposites derived from nanocarbons and layered double hydroxides-properties, synthesis, and applications. Adv Funct Mater 22:675–694
18. Zan X, Bai H, Wang C, Zhao F, Duan H (2016) Graphene Paper decorated with a 2D array of dendritic platinum nanoparticles for ultrasensitive electrochemical detection of dopamine secreted by live cells. Chem 22:5204–5210
19. Asif M, Aziz A, Dao AQ, Hakeem A, Wang H, Dong S, Zhang G, Xiao F, Liu H (2015) Real-time tracking of hydrogen peroxide secreted by live cells using MnO_2 nanoparticles intercalated layered doubled hydroxide nanohybrids. Anal Chim Acta 898:34–41
20. Marcano DC, Kosynkin DV, Berlin JM, Sinitskii A, Sun Z, Slesarev A, Alemany LB, Lu W, Tour JM (2010) Improved synthesis of graphene oxide. ACS Nano 4:4806–4814
21. Shervedani RK, Karevan M, Amini A (2014) Prickly nickel nanowires grown on Cu substrate as a supersensitive enzyme-free electrochemical glucose sensor. Sens Actuat B: Chemical 204:783–790
22. He W, Ding Y, Zhang W, Ji L, Zhang X, Yang F (2016) A highly sensitive sensor for simultaneous determination of ascorbic acid, dopamine and uric acid based on ultra-small Ni nanoparticles. J Electroanal Chem 775:205–211
23. Ma L, Wang Q, Islam SM, Liu Y, Ma S, Kanatzidis MG (2016) Highly selective and efficient removal of heavy metals by layered double hydroxide intercalated with the $MoS_4^{(2-)}$ ion. J Am Chem Soc 138:2858–2866
24. Hu J, Lei G, Lu Z, Liu K, Sang S, Liu H (2015) Alternating assembly of Ni–Al layered double hydroxide and graphene for high-rate alkaline battery cathode. Chem Commun 51:9983–9986
25. Li M, Liu F, Cheng JP, Ying J, Zhang XB (2015) Enhanced performance of nickel–aluminum layered double hydroxide nanosheets/carbon nanotubes composite for supercapacitor and asymmetric capacitor. J Alloys Compd 635:225–232
26. Aziz A, Asif M, Azeem M, Ashraf G, Wang Z, Xiao F, Liu H (2018) Self-stacking of exfoliated charged nanosheets of LDHs and graphene as biosensor with real-time tracking of dopamine from live cells. Anal Chim Acta 65:1–11
27. Ghanbari K, Moloudi M (2016) Flower-like ZnO decorated polyaniline/reduced graphene oxide nanocomposites for simultaneous determination of dopamine and uric acid. Anal Biochem 512:91–102
28. Li B, Zhou Y, Wu W, Liu M, Mei S, Zhou Y, Jing T (2015) Highly selective and sensitive determination of dopamine by the novel molecularly imprinted poly (nicotinamide)/CuO nanoparticles modified electrode. Biosens Bioelectron 67:121–128
29. Ramachandran A, Panda S, Karunakaran Yesodha S (2018) Physiological level and selective electrochemical sensing of dopamine by a solution processable graphene and its enhanced sensing property in general. Sens Actuat B: Chemical 256:488–497
30. Zhao D, Yu G, Tian K, Xu C (2016) A highly sensitive and stable electrochemical sensor for simultaneous detection towards ascorbic acid, dopamine, and uric acid based on the hierarchical nanoporous PtTi alloy. Biosens Bioelectron 82:119–126
31. Zhang D, Li L, Ma W, Chen X, Zhang Y (2017) Electrodeposited reduced graphene oxide incorporating polymerization of l-lysine on electrode surface and its application in simultaneous electrochemical determination of ascorbic acid, dopamine and uric acid. Mater Sci Eng C Mater Biol Appl 70:241–249
32. Thanh TD, Balamurugan J, Lee SH, Kim NH, Lee JH (2016) Effective seed-assisted synthesis of gold nanoparticles anchored nitrogen-doped graphene for electrochemical detection of glucose and dopamine. Biosens Bioelectron 81:259–267
33. Yan X, Gu Y, Li C, Tang L, Zheng B, Li Y, Zhang Z, Yang M (2016) Synergetic catalysis based on the proline tailed metalloporphyrin with graphene sheet as efficient mimetic enzyme for ultrasensitive electrochemical detection of dopamine. Biosens Bioelectron 77:1032–1038
34. Zhang M, Liao C, Yao Y, Liu Z, Gong F, Yan F (2014) High-performance dopamine sensors based on whole-graphene solution-gated transistors. Adv Funct Mater 24:978–985
35. Sudibya HG, Ma J, Dong X, Ng S, Li LJ, Liu XW, Chen P (2009) Interfacing glycosylated carbon nanotube network devices with living cells to detect dynamic secretion of biomolecules. Angew Chem Int Ed 48:2723–2726
36. Li BR, Hsieh YJ, Chen YX, Chung YT, Pan CY, Chen YT (2013) An ultrasensitive nanowire-transistor biosensor for detecting dopamine release from living PC12 cells under hypoxic stimulation. J Am Chem Soc 135:16034–16037